



Adsorption of malic acid at the hydroxyapatite/aqueous NaCl solution interface

Władysław Janusz¹ · Ewa Skwarek¹

Received: 4 May 2021 / Accepted: 7 June 2021 / Published online: 23 June 2021
© The Author(s) 2021

Abstract

The aim of the study was the basic incidence on the phenomenon of adsorption that occurs at the hydroxyapatite/malic acid interface, leading to a change in the surface properties of hydroxyapatite, Analytical methods used in the research: X-ray diffraction (XRD) as well as by the, adsorption–desorption of nitrogen (ASAP), potentiometric titration. The specific adsorption of malic acid ions at the hydroxyapatite interface was investigated by means of the radioisotope method. The zeta potential of hydroxyapatite dispersions was determined by electrophoresis with Zetasizer Nano ZS90 by Malvern. The particle sizes of hydroxyapatite samples were analyzed using Masteriszer 2000 Malvern. Studies on the kinetics of malic acid on hydroxyapatite from a solution with an initial concentration of 1 mmol/dm³ have shown that the adsorption process is initially fast, followed by a slow adsorption step. An increase in the pH of the solution causes a decrease in the malic acid adsorption as a result of competition with hydroxyl ions. The presence of adsorbed malic acid was confirmed by the FTIR measurements. The effect of malic acid adsorption on the zeta potential and particle size distribution of hydroxyapatite in the NaCl solution was investigated.

Keywords Hydroxyapatite · Adsorption · Malic acid

Introduction

Hydroxyapatite, when contacting ions or molecules in the environment in which it is located, changes its properties easily as a result of the adsorption of these components. The systems in which hydroxyapatite interacts with the solutions components is the human body in which hydroxyapatite (HAp) is a mineral component of teeth and bones (Vallet-Regi and Arcos 2016; Jones 2001). Additionally, due to its biocompatibility, hydroxyapatite is used to make ceramics, composites or to cover metal or carbon implants (Okada and Matsumoto, 2015; Bose and Tarafder 2012). In turn, malic acid occurs in foods (this is a component of unripe fruit and it can be added to dishes as an acidity regulator). Malic acid is also produced in the body in the Krebs cycle.

The interactions of carboxylic acids with hydroxyapatite lead to a change in the surface properties of hydroxyapatite

and the decalcification of the surface of hydroxyapatite (e.g. tooth enamel). (Featherstone and Lussi 2006; Fu et al. 2005; Hannig et al. 2005). However, the interactions of high-carboxylic acids with hydroxyapatite are not confined to leaching calcium from the hydroxyapatite surface, but also lead to the sorption of acid anions on the hydroxyapatite surface. This process is complex and depending on the concentration of acid anions in the solution and the pH of the solution, it can take place according to the following mechanisms: ion exchange with hydroxyl groups, phosphate groups as well as in the process of dissolution and recrystallization of hydroxyapatite (Wei et al. 2011; Skwarek et al. 2014; Skwarek 2015; Janusz and Skwarek 2020). It was found that the adsorption of polycarboxylic acids (citric, tartaric) anions on the crystal walls forming the hydroxyapatite surface is not the same, which leads to a different growth rate of individual walls of the hydroxyapatite crystal, as a result of the formation of hydroxyapatite crystals of different morphology (Filgueiras et al. 2006; Gopi et al. 2013). A similar effect was found due to the synthesis in the presence of malic acid (Gopi et al. 2015).

The literature reports a paper presenting the results of studies on the adsorption of polycarboxylic acids on

✉ Ewa Skwarek
ewunias@hektor.umcs.lublin.pl

¹ Department of Radiochemistry and Environmental Chemistry, Faculty of Chemistry, Maria Curie-Skłodowska University, Lublin, Poland

hydroxyapatite, which relate to oxalic and citric acids. Malic acid adsorption studies were carried out as comparative studies with oxalic and citric acids using the hydroxyapatite samples with varying degrees of crystallinity. Adsorption was tested in the concentration range of polycarboxylic acids 0.5–10 mmol/dm³, in the range of pH 2–10, in a solution of 5 mmol/dm³ KCl using the method of substance uptake from solution. It was found that in this range of acid concentrations adsorption decreases with the increasing pH, and the adsorption isotherm is described by the Freundlich equation. The research presented in this paper concerns relatively high concentrations of carboxylic acid ions > 0.5 mmol/dm³ and the pH range in which hydroxyapatite dissolves to a great extent at pH < 4.

The paper presents the investigations on the kinetic and static adsorption of malate ions at the hydroxyapatite using ¹⁴C radiolabelled malic acid from the solutions with malic acid of the initial concentration from 1 μmol/dm³ to 1 mmol/dm³ and pH range from 6 to 11 in the 1 mmol/dm³ aqueous solution of NaCl. The adsorption measurements were completed by the spectrometric, potentiometric titration of HAp suspensions as well as the electrophoretic measurements of zeta potential and particle size analysis using the static light scattering method.

Experimental

Materials and methods

The studies of malate ions adsorption on hydroxyapatite were carried out using the commercial sample of hydroxyapatite supplied by Aldrich. Hydroxyapatite was characterized using X-ray diffraction (XRD).

Comparison of the surface and porosity of hydroxyapatite before and after adsorption of malic acid was carried out on the basis of data from the analysis of nitrogen adsorption/desorption isotherms obtained with the ASAP2405-Accelerated Surface Area and Porosimetry apparatus, Micromeritics Instruments, Co. Before the measurement of nitrogen adsorption, the samples were degassed in a temperature 50 °C for 2 h. The specific surface area of the samples was calculated based on the nitrogen adsorption isotherm by the BET method. The porosity of the samples was characterized by the BJH method from the nitrogen desorption isotherm.

The specific adsorption of malic acid ions at the hydroxyapatite interface was investigated by means of the radioisotope method as a function of malic acid ions and concentration, as well as NaCl and pH. The initial concentration of malic acid ions ranged from 1 μmol/dm³ to 1 mmol/dm³, pH was changed from 6 to 12. As a background electrolyte NaCl solution was used of the concentration 1 mmol/dm³. The adsorption measurements were completed by the

potentiometric titration of hydroxyapatite suspensions and electrophoresis measurements.

To remove ionic type contamination, which might influence the ion adsorption measurements, hydroxyapatite was washed with doubly distilled water until constant conductivity (~ 10 μS/cm was achieved). Adsorption and surface charge measurements were made simultaneously in the suspension of the same solid content to maintain the identical conditions of the experiments in a thermostated Teflon vessel at 25 °C. To eliminate the influence of CO₂ all potentiometric and adsorption measurements were performed in the nitrogen atmosphere. The pH values were measured using a set of glass REF 451 and calomel pHG201-8 electrodes with the Radiometer assembly. The surface charge density was calculated from the difference of the amounts of added acid or base to obtain the same pH value of suspension as for the background electrolyte.

The zeta potential of hydroxyapatite dispersions was determined by electrophoresis with Zetasizer Nano ZS90 by Malvern. The measurements were performed at 100 ppm solid concentration ultrasonication of the suspension. The particle sizes of hydroxyapatite samples were analyzed using Masteriszer 2000 Malvern.

Results and discussion

The pH range in which the interactions of malic acid with hydroxyapatite were studied was limited due to the solubility of hydroxyapatite from pH = 6 to pH = 11. Taking into account the values of phosphoric acid dissociation constants pK_{a1} = 2.16, pK_{a2} = 7.21 and pK_{a3} = 12.32 (Linede 2003) and those of the dissociation constants of malic acid pK_{a1} = 3.03 and pK_{a2} = 4.37 (Martel and Smit 1989) in the studied pH range, (Fig. 1), up to pH = 7, the phosphate anion form will dominate, while above the phosphate anion will dominate. However, throughout this pH range, malic acid will be present in the form of malate anion.

Considering the ionic forms that dominate in the studied pH range in the interactions of malate anions, exchanging these anions with hydrogen phosphate, phosphate or hydroxyl ions in the hydroxyapatite crystal lattice can be taken into account. In addition, the adsorption of malate anions on the hydroxyl groups contributes to the formation of exterior spherical complexes as well as dissolution and recrystallization processes. In the crystal structure of hydroxyapatite there are natural type I channels with (Solhy et al. 2011). The second type of channel allows ion exchange, but the exchange process will be limited by diffusion inside this channel.

Figure 2 presents the kinetics of malate ion adsorption on hydroxyapatite from a solution of the initial concentration of

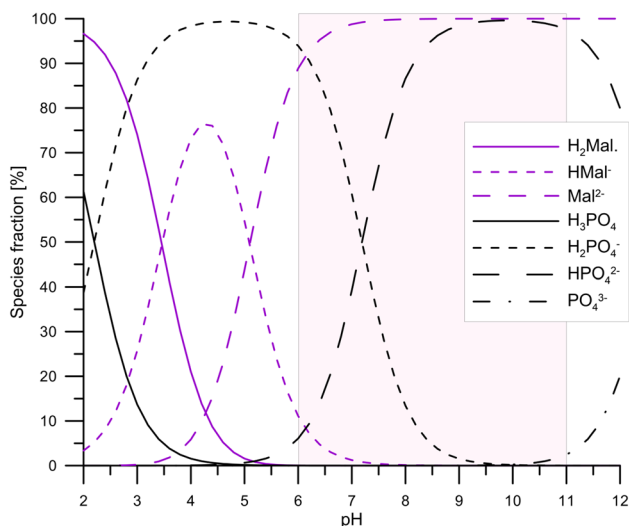


Fig. 1 The comparison of Malic (Mal) and phosphate forms as a function of pH in the aqueous solutions. The rectangle denotes the experimental pH range

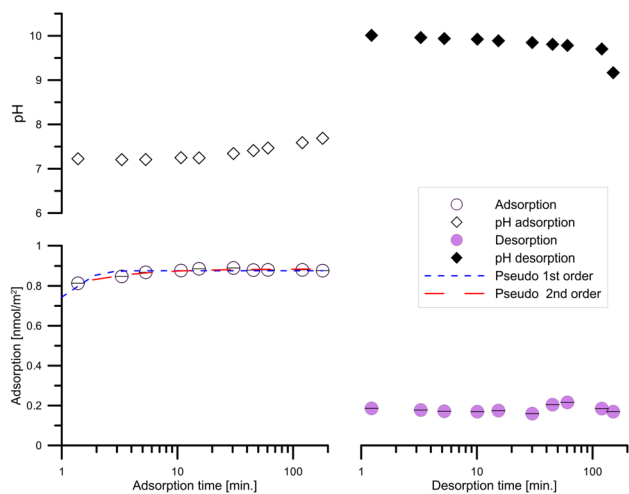


Fig. 2 Kinetics of pH and malic ions adsorption/desorption changes on hydroxyapatite from the malic ions solution of the initial concentration $1 \mu\text{mol}/\text{dm}^3$. The points indicate the experimental data, the broken line-the pseudo-first-order model for $q_e=0.876 \text{ nmol}/\text{m}^2$ and $k_1=1.89$, the broken line of longer segments- the pseudo-second-order model for $q_e=0.885 \text{ nmol}/\text{m}^2$ and $k_2=9.27$

$1 \mu\text{mol}/\text{dm}^3$ and pH changes. In addition, Fig. 2. shows the kinetics of malate ion desorption after a change at $\text{pH}=10.0$. As can be seen, adsorption of malate ions from a solution with an initial concentration of $1 \mu\text{mol}/\text{dm}^3$ occurs rapidly and practically settles within 10 min (88% of malate ions is adsorbed). The course of adsorption as a function of time is slightly better described by the pseudo-second-order equation than the pseudo first-order one. After increasing the suspension pH to $\text{pH}=10$, desorption of malate ions to $\sim 18\%$ of the total amount of ions in the system is observed. After

this change in the pH, value its drift towards lower values is observed, initially a slight pH drift towards lower values, and after 100 min more rapid to $\text{pH}=9.2$. After 30 min. an increase in malate ion adsorption to 21.8% is observed, followed by a further decline to 17%.

The kinetics of adsorption/desorption of malate ions from a solution with an initial concentration of $1 \mu\text{mol}/\text{dm}^3$ on hydroxyapatite is similar to that of tartrate ions (Janusz and Skwarek 2020).

The kinetics of malate ion adsorption on hydroxyapatite and the change of pH during adsorption and desorption of malate ions after increasing the $\text{pH}=10.07$ are shown in Fig. 3. The kinetics of malate ion adsorption is complex, after a quick adsorption step during the first 10 min of contact of the hydroxyapatite with the initial concentration solution $1 \text{ mmol}/\text{dm}^3$ of malate ions (58% of total malate ions is adsorbed), a slow adsorption increase takes up to 1000 min (66% of ions is adsorbed), adsorption increases still recorded up to 10,080 min, where adsorption increases to 90% of the total amount of malate ions in the system. An increase in pH to 10.07 causes a decrease in adsorption to 82%, after which over time there is a slow decrease in adsorption of malate ions within 30 min to 80% and a decrease in $\text{pH}=9.6$. After 45 min, the suspension pH decreases further to reach 7.96 after 80 min but during this time the adsorption of malate ions increases and reaches 100% of the total amount of malate ions in the system. This course of adsorption means that the pseudo-first and the pseudo-second-order kinetics models are not able to describe experimentally the changes in adsorption observed over time (Marczewski 2007). A good fit was achieved using only a multiexponential model (Derylo-Marczewska et al. 2010). The fast adsorption process is associated with the ion exchange reactions on the hydroxyapatite surface. However, the third stage, connected with a significant increase in adsorption may be a result of malate ions diffusion into the hydroxyapatite crystal structure through type II channels. Similar to the kinetics of adsorption/desorption of malate ions from a solution with an initial concentration of $1 \mu\text{mol}/\text{dm}^3$ on hydroxyapatite, also in the case of the kinetics of adsorption/desorption from a solution with an initial concentration of $1 \text{ mmol}/\text{dm}^3$, the behavior is similar to that of tartrate ions with the same initial concentration (Janusz and Skwarek 2020).

The relationship between the adsorption and the changes in the concentration of malate ions on hydroxyapatite as a function of pH from a solution with the initial concentrations of malate ions $1 \mu\text{mol}/\text{dm}^3$ and $1 \text{ mmol}/\text{dm}^3$ is presented in Figs. 4 and 5, respectively. For an initial concentration of malate ions $1 \mu\text{mol}/\text{dm}^3$, (Fig. 3), 88% of the total amount of malate ions in the system is adsorbed from the solution at $\text{pH}=7$. As the pH increases, the adsorption decreases and at $\text{pH}=10.9$ the adsorption drops to 10.5%. Adsorption of malate ions from a solution with an initial concentration

Fig. 3 Kinetics of pH and malate ions adsorption/desorption changes on hydroxyapatite from the malate ions solution of the initial concentration 1 mmol/dm^3 . The points indicate the experimental data, the broken line-the pseudo-first-order model for $q_e=0.64 \text{ } \mu\text{mol/m}^2$ and $k_1=0.73$, the broken line of longer segments- the pseudo-second-order model for $q_e=0.67 \text{ } \mu\text{mol/m}^2$ and $k_2=1.64$. The continuous line the multiexponential model: $a_{\text{eq}}=0.946$, $A_0=0.714$, $k_1=2.48$, $A_1=0.0024$, $k_2=2.28 \times 10^{-4}$, $A_2=0.108$, $k_3=0.903$, $A_3=0.175$

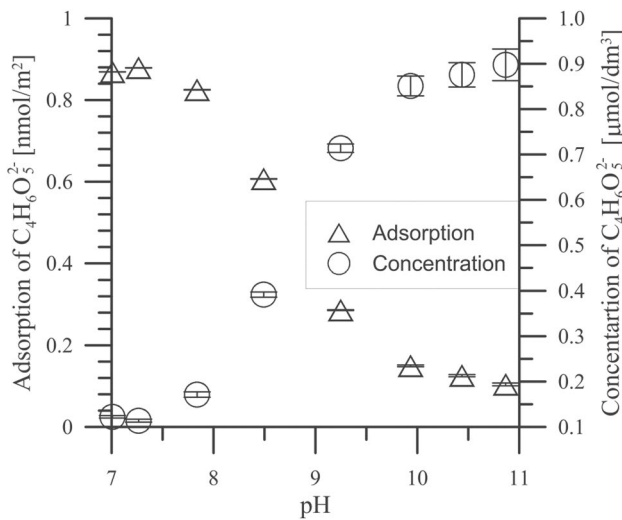
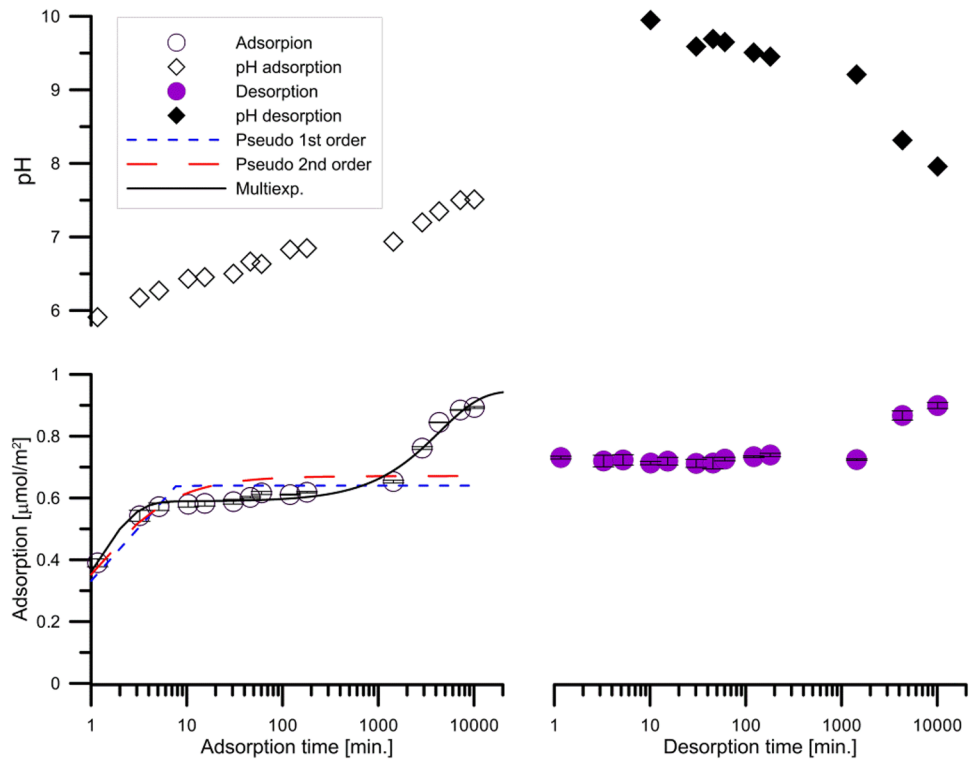


Fig. 4 Dependence of adsorption density and concentration of malate ions on pH for the hydroxyapatite/ $1 \text{ mmol/dm}^3 \text{ NaCl} + 1 \text{ } \mu\text{mol/dm}^3$ malate ions

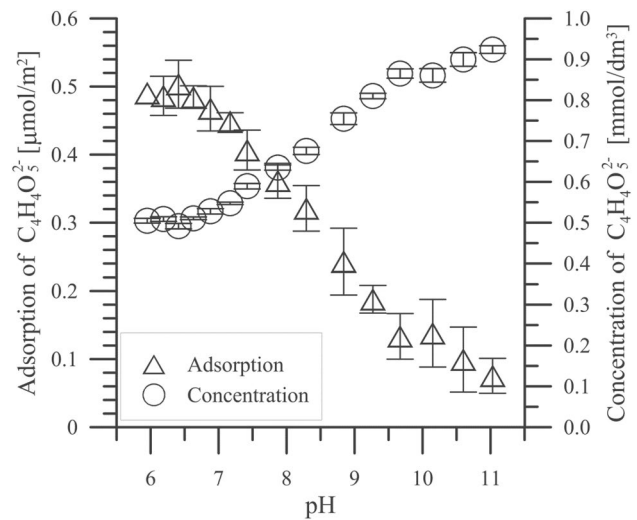


Fig. 5 Dependence of adsorption density and concentration of malate ions on pH for the hydroxyapatite/ $1 \text{ mmol/dm}^3 \text{ NaCl} + 1 \text{ mmol/dm}^3$ malate ions

of 1 mmol/dm^3 also decreases with the increasing pH of the solution. However, at $\text{pH}=6$, approx. 50% of the initial concentration of malate ions is adsorbed, and at $\text{pH}=10.6$, 10% is adsorbed.

However, in the case of anion adsorption in the metal oxide systems, electrolyte solution, the anion adsorption

is characterized by adsorption envelope and decreases in the pH range from $\sim 100\%$ to $\sim 0\%$ (Janusz and Matysek 2006). Unlike insoluble metal oxides with a surface having hydroxyl functional groups, the hydroxyapatite surface is more complex, possessing hydroxyl, hydrogen phosphate and calcium ions (Kukura et al. 1973).

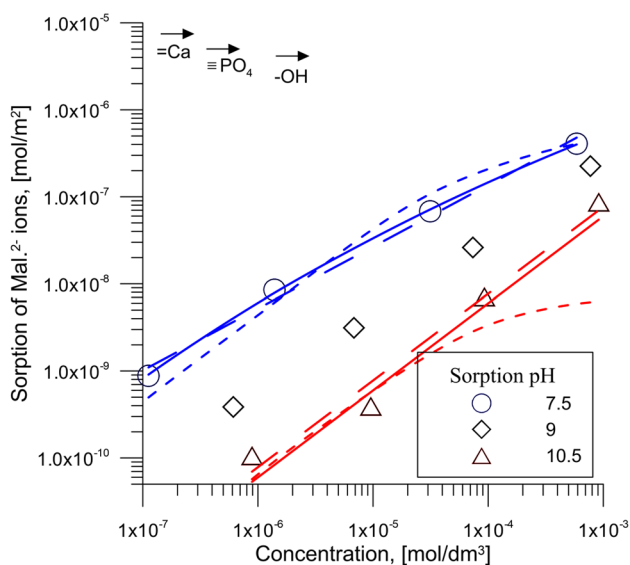


Fig. 6 Dependence of adsorption density and concentration of malate ions on pH for the hydroxyapatite/0.001 mol/dm³ NaCl+0.000001 mol/dm³ malate ions system. The short dash line—indicates the Langmuir isotherm fit, the long dash line—the Freundlich isotherm fit, the solid line—the Redlich-Patterson isotherm fit

Figure 6 shows the dependence of malate ion adsorption on hydroxyapatite as a function of the equilibrium concentration of malate ions at pH = 7.5, 9 and 10.5. Figure 6 presents the adsorption levels corresponding to the adsorption on the active groups of hydroxyapatite surfaces, i.e. Ca²⁺ ions, hydroxyl and hydrogen phosphate groups. These amounts were calculated on the basis of the data calculated the amount of relevant atoms falling on the walls of the hydroxyapatite crystal cells exposed on its surface (Kukura et al. 1973; Skartsila and Spanos 2007; Bertinetti et al. 2007). As can be seen adsorption of malate ions from a solution with an initial concentration of 1 mmol/dm³ does not exceed the formal monolayer coverage of any of the adsorption sites. The Langmuir, Freundlich and Redlich-Patterson adsorption equations were fitted to the experimental data of malate ion adsorption presented in Fig. 6. The parameters from the nonlinear fit of the Langmuir and Redlich-Patterson isotherms matching and the log (adsorption) log (concentration) fit for the Freundlich isotherm are given in Table 1.

The isotherms dependence calculated based on the relevant parameters isotherms dependence is given in Fig. 6. The short dash line—the Langmuir isotherm fit, the long dash line—Freundlich isotherm fit, solid line—the Redlich-Patterson isotherm fit. The presented data indicate that the dependence of malate ion adsorption has hydroxyapatite as a function of the equilibrium concentration of malate ions at pH = 7.5 is best described by the Redlich-Patterson isotherm (Redlich and Peterson 1959), while at pH = 9 and 10.5 by the Freundlich isotherm.

Table 1 Parameters of Langmuir, Freundlich and Redlich-Patterson isotherms for the adsorption of malate ions on the hydroxyapatite surface

Parameters	Unit	pH		
		7.5	9	11
Langmuir				
<i>a_m</i>	mol/m ²	1.14 × 10 ⁻⁶	5.69 × 10 ⁻⁷	5.54 × 10 ⁻⁸
<i>K_L</i>	dm ³ /mol	1664.5	798.0	1039.2
MPSD	%	78.2	25.1	70.2
<i>R</i> ²		0.903	0.997	0.195
Freundlich				
<i>K_F</i>	(mol ^(1-1/n))dm ^{3/n} /m ²	9.36 × 10 ⁻⁵	1.30 × 10 ⁻⁴	7.47 × 10 ⁻⁵
<i>n</i>		1.410	1.122	1.004
MPSD	%	28.1	4.3	68.8
<i>R</i> ²		0.970	0.999	0.993
Redlich-Patterson				
<i>K_{RP}</i>	dm ³ /m ²	9.98 × 10 ⁻³	4.65 × 10 ⁻⁴	5.98 × 10 ⁻⁵
<i>α_{RP}</i>	(dm ³ /mol) ^{β_{RP}}	474.2	463.4	0.1
<i>β_{RP}</i>		0.477	0.905	1
MPSD	%	10.2	34.6	80.1
<i>R</i> ²		0.999	0.994	0.739

a_e—the experimental adsorption, *a_c*—the calculated adsorption, *MPSD* Marquardt’s Percent Standard Deviation (Simsek and Beker 2014), *R*²—the coefficient of determination (Simsek and Beker 2014)

$$a_c = \frac{a_m K_L c_e}{1 + K_L c_e}$$

where: *a_c* (mol/m²)—adsorption of malate ions, *c_e*—the equilibrium concentration of malate ions, *a_m*—the maximum amount of the malate ions, *K_L*—the constant related to the binding energy,

$$a_c = K_F c_e^{1/n}$$

where *K_F* and 1/*n*—are the empirical constants of the Freundlich isotherm.

$$a_{exp} = \frac{K_{RP} C \exp}{1 + \alpha_{RP} C^{\beta_{RP}}}$$

K_{RP}—the Redlich-Peterson isotherm constant, *α_{RP}*—the Redlich-Peterson isotherm constant, *β_{RP}*—the exponent varies from 0 to 1.

Figure 7 shows the difference in the FTIR spectra of hydroxyapatite and hydroxyapatite with adsorbed malic acid from a solution with an initial concentration of 1 mmol/dm³. The analysis of absorption bands in the spectrum presented in Fig. 8 and the wavenumbers obtained for them are given in column 1 of Table 2. A comparison of the determined values of wavenumbers with the literature data indicates that most characteristic bands correspond

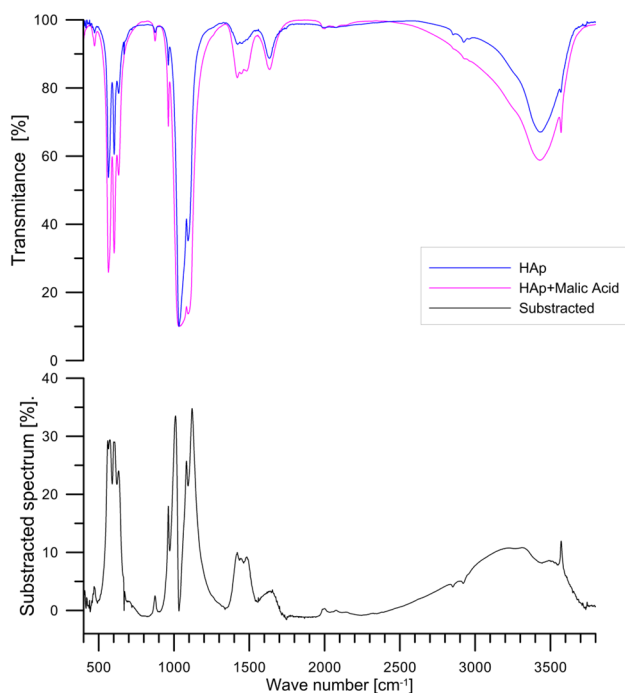


Fig. 7 FTIR spectrum of malic acid adsorbed on hydroxyapatite

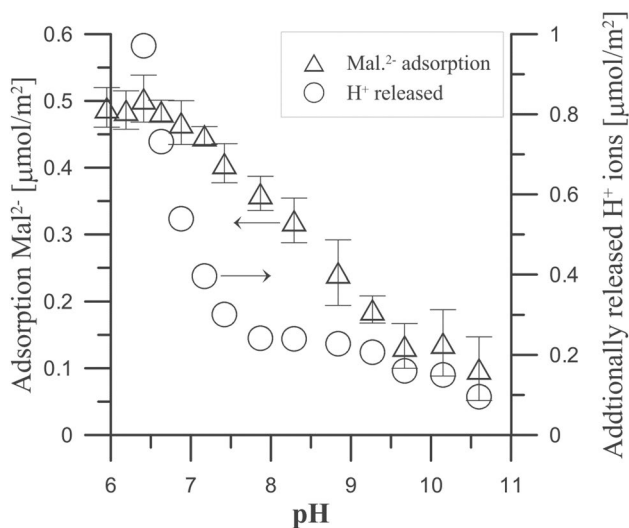


Fig. 8 Comparison of adsorption density of malate ions on hydroxyapatite and released hydrogen ions

to DL malic acid (Baranska et al. 2003). A spectrum of carbonate characteristic band appears at 1484 cm^{-1} that may have caused CO_2 adsorption during the sample preparation. However, the band at the wavenumber corresponds to the bending vibrations of the OH group caused by the presence of water associated with HAp (Koutsopoulos 2002).

To determine the mechanism of ion adsorption on hydroxyapatite, adsorption of malate ions and the amount of H^+ ions released as a result of malate adsorption determined based on the potentiometric titration were compared. The amount of hydrogen ions released as a result of malic acid adsorption was calculated by subtracting the dependence of the released ions calculated from the hydroxyapatite titration curve in the presence of malic acid from the hydroxyapatite titration curve. The dependence of malate ions adsorption additionally results in hydrogen ion release which is shown in Fig. 8. As can be seen in the $\text{pH} < 7$ range one adsorbing malate ion releases two hydrogen ions, above $\text{pH} 7$, one hydrogen ion is statistically released about by the adsorbed malate ion. As a result of malate ions adsorption on the surface, the concentration of negatively charged groups increases. This effect can be explained by the exchange of hydroxyl groups with malic acid anions which have a stronger acidic character than the hydroxyl group.

The effect of malate ion adsorption on the dependence of the zeta potential as a function of pH hydroxyapatite in a solution of 1 mmol/dm^3 NaCl is presented in Fig. 9. The presence of malate ions with an initial concentration of $1\text{ }\mu\text{mol/dm}^3$ in the system hydroxyapatite/ 1 mmol/dm^3 NaCl solution, practically does not differ from the dependence of the zeta potential as a function of pH in the absence of malate ions in the above concentration. Adsorption of malate ions from a solution with an initial concentration of 0.1 mmol/dm^3 in the pH range > 7.5 causes a stronger decrease in the zeta potential with an increase in pH than in the absence of malate ions in solution. This effect may be associated with a change in the sorption mechanism of malate ions. Instead of replacing phosphate ions the exchange of hydroxyl ions, which have a weaker acidic nature than malate ions, may take place. The presence of malate ions at the initial concentration of 1 mmol/dm^3 in the pH range < 7.5 causes a decrease in the zeta potential due to the exchange of ions with weaker acidic character on the surface of hydroxyapatite for malate ions with stronger acidic character. However, a further increase of pH causes an increase in the zeta potential due to the desorption of malate ions with an increase of pH and chemical changes in the surface composition.

Comparison of the specific surface area and porosity of the hydroxyapatite sample conditioned in a 1 mmol/dm^3 NaCl solution with the HAp sample conditioned in a mixture of 1 mmol/dm^3 NaCl with 1 mmol/dm^3 malic acid is shown in Table 3, while the pore distribution as a partial surface dependence on the log diameter is shown in Fig. 10. The data presented in Table 3 indicate that in the presence of malic acid there is a decrease in the specific surface area of the sample mainly due to the decrease in the micropore surface area (t-plot data). Nevertheless, the pore volume determined by the BJH method is similar. The relationships

Table 2 Observed wavenumbers (cm⁻¹) and assignments for malic acid on the hydroxyapatite surface

Experimental cm ⁻¹	Ref. cm ⁻¹	Assignment	Ref
3572	3593	$\nu(\text{OH}^-)$	(Diallo-Garcia et al. 2018)
3490	3445	$\nu(\text{OH})$ of CHOH	(Baranska et al. 2003)
2837	2847	Hydrogen bonding	(Baranska et al. 2003)
1654	1639	(OH)	(Koutsopoulos 2002)
1484	1461	$\nu(\text{CO}_3^{2-})$	(Diallo-Garcia et al. 2018)
1444	1436	$\delta(\text{CH}_2)_{\text{scis}}$	(Baranska et al. 2003)
1420	1399	$\nu(\text{CO})$	(Baranska et al. 2003)
1120	1106	$\delta(\text{CH}_2)_{\text{scis}}, \nu(\text{C-O}), \delta(\text{OH})$	(Baranska et al. 2003)
1083			
1010	1034	$\nu(\text{C-C}), \gamma(\text{CH})$	(Baranska et al. 2003)
962	958	$\nu(\text{C-C}), (\text{C-O})_{\text{tors}}$	(Baranska et al. 2003)
874	887	$\delta(\text{C-O}), \nu(\text{C-CH}_2), \delta(\text{C-H})$	(Baranska et al. 2003)
632	635	$\delta(\text{OH}), \delta(\text{CH}_2), \nu(\text{C-C})$	(Baranska et al. 2003)
600		Hydrogen bonding	(Baranska et al. 2003)
575			
560	529	$\delta(\text{COO}), \delta(\text{C-H}), \nu(\text{C-C})$	(Baranska et al. 2003)
470	472	$\delta(\text{C-H}), \delta(\text{COO})_{\text{rock}}$	(Baranska et al. 2003)

δ_{twist} —the twisting deformation, δ_{rock} —the rocking deformation, δ_{wagging} —the wagging deformation, δ_{scis} —the scissors deformation, ν —the stretching, δ —the deformation, tors.—the torsion

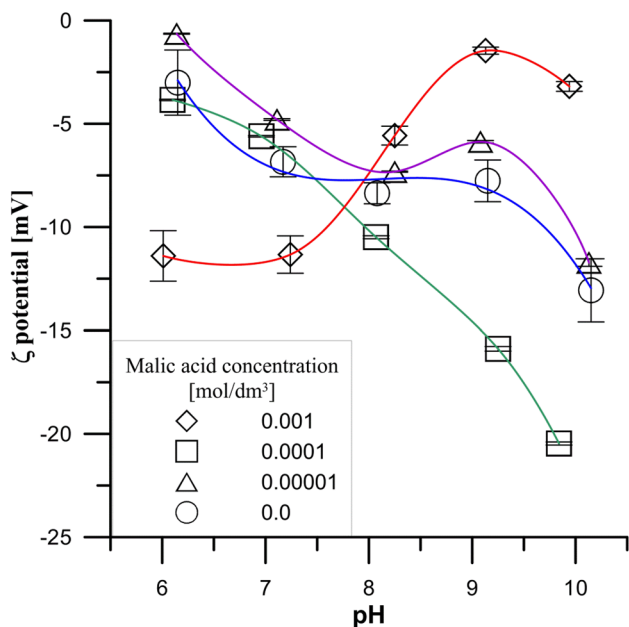


Fig. 9 Effect of malate ion adsorption on HAp on the zeta potential as a function of solution pH

presented in Fig. 10 show that the presence of malic acid causes an decrease in the proportion of incremental volume mesopores in the range from 7.6 nm to 22 nm and a increase in the proportion of mesopores in the pore diameter above 22 nm.

A comparison of the effect of malate ions on the particle size distribution of hydroxyapatite conditioned in the

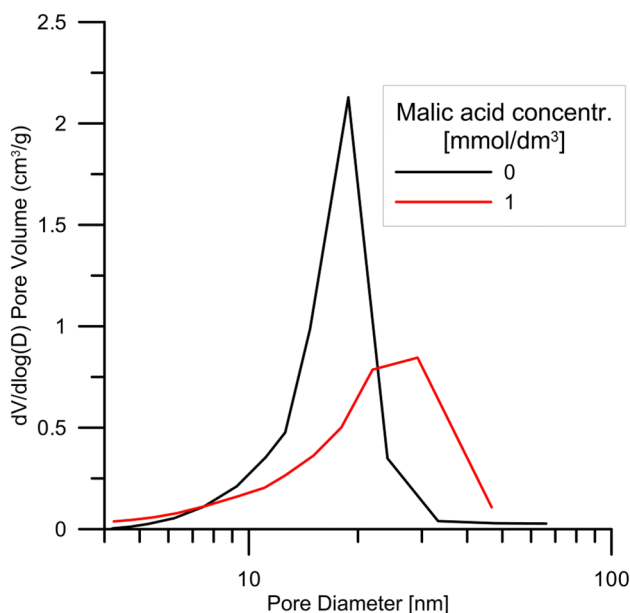
1 mmol/dm³ NaCl solution + 1 mmol/dm³ malate ions with appropriate conditioning in the 1 mmol/dm³ NaCl solution indicates that the distribution of particle size of hydroxyapatite occurs affected by the malate ion adsorption, Fig. 11. It consists of reducing the proportion of fractions from 0.5 to 9 μm, increasing the fraction with a grain size from 9 to 50 μm and disappearance of the fraction from 50 to 300 μm (breaking up aggregates). On one hand, this effect can be caused by the weak electrostatic interactions (in the pH range < 7.5 $\zeta \cong 10$ mV) and the ultrasound during the grain size distribution measurements which can lead to the breakdown of large aggregates and combining of small particles into larger ones.

Conclusions

Studies on the kinetics of malate ion adsorption on hydroxyapatite from a solution of initial concentration of 1 μmol/dm³ showed that the adsorption equilibrium is reached within 10 min and the kinetics of the adsorption is well described by the pseudo second-order model. However, the adsorption kinetics of malate ions from a solution with an initial ion concentration of 1 mmol/dm³ is more complex, it takes more time to reach the adsorption equilibrium, and the process is well described in a multi-exponential model. An increase in pH from 6 to 11 causes a decrease in the adsorption of malate ions on hydroxyapatite and indicates a competitive exchange of malate ions for hydroxyl ions in hydroxyapatite. This mechanism is confirmed by the increase

Table 3 Parameters characterizing the specific surface area and porosity of hydroxyapatite samples

Property	HAP/0.001 mol/dm ³ NaCl	HAP/0.001 mol/dm ³ Malate
BET surface area (m ² /g)	97.9	96.5
Langmuir surface area (m ² /g)	143.0	141.7
t-plot micropore area (m ² /g)	10.2	5.2
t-plot external surface area (m ² /g)	87.7	91.3
BJH Adsorption cumulative volume of pores 1.7 nm < d < 300 nm diameter (cm ³ /g)	0.47	0.45
BJH Desorption cumulative volume of pores 1.7 nm < d < 300 nm diameter (cm ³ /g)	0.46	0.46
Adsorption average pore width (4 V/A by BET) (nm)	19.4	18.9
BJH Adsorption average pore diameter (4 V/A) (nm)	19.1	18.2
BJH Desorption average pore diameter (4 V/A) (nm)	16.0	16.0

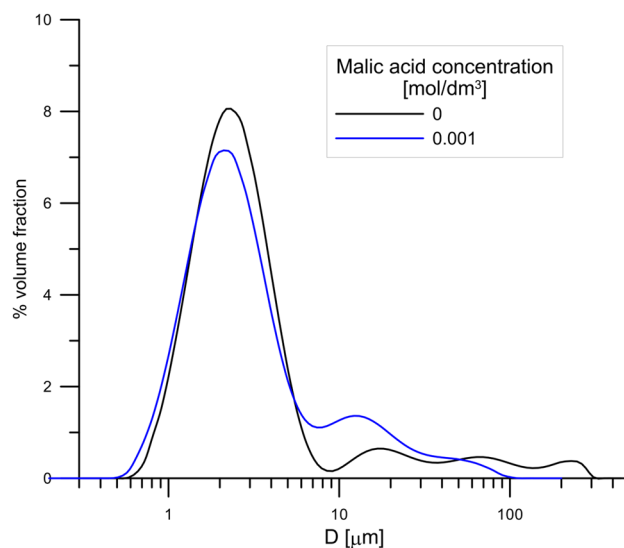
**Fig. 10** Differential pore volume distribution of HAp samples

in acidity of the groups on the surface of hydroxyapatite due to the adsorption of malate ions.

Declarations

Conflict of interest The authors declare that they have no known competing financial interests or personal relationships that could have appeared to influence the work reported in this paper.

Open Access This article is licensed under a Creative Commons Attribution 4.0 International License, which permits use, sharing, adaptation, distribution and reproduction in any medium or format, as long as you give appropriate credit to the original author(s) and the source, provide a link to the Creative Commons licence, and indicate if changes were made. The images or other third party material in this article are included in the article's Creative Commons licence, unless indicated otherwise in a credit line to the material. If material is not included in the article's Creative Commons licence and your intended use is not

**Fig. 11** Effect of malate ion adsorption on the particle size distribution of hydroxyapatite after its conditioning in the 1 mmol/dm³ NaCl and 1 mmol/dm³ NaCl + 1 mmol/dm³ malic acid solutions

permitted by statutory regulation or exceeds the permitted use, you will need to obtain permission directly from the copyright holder. To view a copy of this licence, visit <http://creativecommons.org/licenses/by/4.0/>.

References

- Baranska H, Kuduk-Jaworska J, Szostak R, Romaniewska A (2003) Vibrational spectra of racemic and enantiomeric malic acids. *J Raman Spectrosc* 34:68–76
- Bertinetti L, Tampieri A, Landi E, Ducati C, Midgley PA, Coluccia S, Martra G (2007) Surface structure, hydration, and cationic sites of nanohydroxyapatite: UHR-TEM, IR, and microgravimetric studies. *J Phys Chem C* 111:4027–4038

- Bose S, Tarafder S (2012) Calcium phosphate ceramic systems in growth factor and drug delivery for bone tissue engineering: a review. *Acta Biomater* 8:1401–1421
- Derylo-Marczewska A, Marczewski AW, Sz W, Sternik D (2010) Studies of adsorption equilibria and kinetics in the systems: aqueous solution of dyes -mesoporous carbons. *Appl Surf Sci* 256:5164–5170
- Diallo-Garcia S, Ben Osman M, Krafft JM, Casale S, Thomas C, Kubo J, Costentin G (2018) Identification of surface basic sites and acid–base pairs of hydroxyapatite. *J Phys Chem C* 118:12744–12757
- Featherstonea JDB, Lussi A (2006) Understanding the chemistry of dental erosion. In (ed): dental erosion. (A. Lussi ed.) *Monogr Oral Sci*. Basel, Karger 20:66–76
- Filgueiras MRT, Mkhonto D, de Leeuw NH (2006) Computer simulations of the adsorption of citric acid at hydroxyapatite surfaces. *J Cryst Growth* 294:60–68
- Fu B, Shen Q, Qian W, Zeng Y, Sun X, Hannig M (2005) Interfacial interaction of tartaric acid with hydroxyapatite and enamel. *J Mater Sci-Mater Med* 16:827–831
- Gopi D, Bhuvaneshwari N, Indira J, Kanimozhi K, Kavitha L (2013) A novel green template assisted synthesis of hydroxyapatite nanorods and their spectral characterization. *Spectrochimica Acta Part A* 107:196–202
- Gopi D, Bhuvaneshwari N, Kavitha L, Ramya S (2015) Novel malic acid mediated green route for the synthesis of hydroxyapatite particles and their spectral characterization. *Ceram Int* 41:3116–3127
- Hannig Ch, Hamkens A, Becker K, Attin R, Attin T (2005) Erosive effects of different acids on bovine enamel: release of calcium and phosphate in vitro. *Arch Oral Biol* 50:541–552
- Janusz W, Matysek M (2006) Coadsorption of Cd(II) and oxalate ions at the TiO₂/electrolyte solution interface. *J Coll Interface Sci* 296:22–29
- Janusz W, Skwarek E (2020) Comparison of oxalate, citrate and tartrate ions adsorption in the hydroxyapatite/aqueous electrolyte solution system. *Coll Interfaces* 4:45–54
- Jones FH (2001) The teeth and bones: applications of surface science to dental materials and related biomaterials. *Surf Sci Rep* 42(3):75–205
- Koutsopoulos S (2002) Synthesis and characterization of hydroxyapatite crystals: a review study on the analytical methods. *J Biomed Mater Res* 62:600–612
- Kukura M, Bell LC, Posner AM, Quirk JP (1973) Radioisotope determination of the surface concentrations of calcium and phosphorus on hydroxyapatite in aqueous solution. *J Phys Chem* 76:900–904
- Linde DR (ed) (2003) *Handbook of chemistry and physics*, 84th edn. CRC Press, Boca Raton, FL
- Marczewski AW (2007) Kinetics and equilibrium of adsorption of organic solutes on mesoporous carbons. *Appl Surf Sci* 253:5818–5826
- Martel AE, Smit RM (1989) *Critical stability, constants second supplement*, vol 6. Springer Science
- Okada M, Matsumoto T (2015) Synthesis and modification of apatite nanoparticles for use in dental and medical applications. *Jap Dent Sci Rev* 51:85–95
- Redlich O, Peterson DL (1959) A useful adsorption isotherm. *J Phys Chem* 63:1024
- Simsek EB, Beker U (2014) Equilibrium arsenic adsorption onto metallic oxides: isotherm models, error analysis and removal mechanism. *Korean J Chem Eng* 31:2057–2069
- Skartsila K, Spanos N (2007) Surface characterization of hydroxyapatite: potentiometric titrations coupled with solubility measurements. *J Coll Interface Sci* 308:405
- Skwarek E, Janusz W, Sternik D (2014) Adsorption of citrate ions on hydroxyapatite synthesized by various methods. *J Radioanal Nucl Chem* 299:2027–2036
- Skwarek E (2015) Thermal analysis of hydroxyapatite with adsorbed oxalic acid. *J Therm Anal Calorim* 122(1):33–45
- Solhy A, Amara W, Karkouri M, Tahir R, El Bouarib A, Fihri A, Bousmina M, Zahouily M (2011) Bi-functional modified-phosphate catalyzed the synthesis of - α , α -(EE)-bis(benzylidene)-cycloalkanones: microwave versus conventional-heating. *J Mol Catal a: Chem* 336:8–15
- Vallet-Regi M, Arcos Navarrete D (2016) Biological apatites in bone and teeth, in nanoceramics in clinical use: from materials to applications. *Royal Soc Chem Nanosci Nanotechnol* 39:1–29
- Wei W, Zhang X, Cuia J, Wei Z (2011) Interaction between low molecular weight organic acids and hydroxyapatite with different degrees of crystallinity. *Colloids Surf, A* 392:67–75